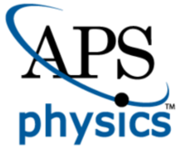

CHORUS

This is the accepted manuscript made available via CHORUS. The article has been published as:

First-principles studies of electric field effects on the electronic structure of trilayer graphene

Yun-Peng Wang, Xiang-Guo Li, James N. Fry, and Hai-Ping Cheng

Phys. Rev. B **94**, 165428 — Published 21 October 2016

DOI: 10.1103/PhysRevB.94.165428

First-principles studies of electric field effects on the electronic structure of trilayer graphene

Yun-Peng Wang, Xiang-Guo Li, James N. Fry, and Hai-Ping Cheng
Quantum Theory Project and Department of Physics,
University of Florida, Gainesville, Florida 32611, USA

A gate electric field is a powerful way to manipulate the physical properties of nano-junctions made of two-dimensional crystals. To simulate field effects on the electronic structure of trilayer graphene, we used density functional theory in combination with the effective screening medium method, which enables us to understand the field-dependent layer-layer interactions and the fundamental physics underlying band gap variations and the resulting band modifications. Two different graphene stacking orders, Bernal (or ABC) and rhombohedral (or ABA) were considered. In addition to confirming the experimentally observed band gap opening in ABC-stacked and the band overlap in ABA-stacked trilayer systems, our results reveal rich physics in these fascinating systems, where layer-layer couplings are present but some characteristics features of single-layer graphene are partially preserved. For ABC stacking, the electric-field-induced band gap size can be tuned by charge doping, while for ABA band the tunable quantity is the band overlap. Our calculations show that the electronic structures of the two stacking orders respond very differently to charge doping. We find that in the ABA stacking hole doping can reopen a band gap in the band-overlapping region, a phenomenon distinctly different from electron doping. The physical origins of the observed behaviors were fully analyzed, and we conclude that the dual-gate configuration greatly enhances the tunability of the trilayer systems.

I. INTRODUCTION

Ultra-thin graphite thin films have great potential for applications in nanoelectronics.[1,2] Many of these applications require a sizable band gap, a feature that is lacking in graphene monolayers.[3] Bilayer graphene with Bernal stacking order exhibits a band gap tunable by controlling the electric field perpendicular to the graphene sheet.[4–6] The two thermodynamically stable rhombohedral (ABC) and Bernal (ABA) stacking orders of trilayer graphene, as shown in Figs. 1(a,b), have been extensively studied in experiments measuring electrical transport properties,[7–9] infrared conductivity,[10] and scanning tunneling spectroscopy,[11] and exhibit very different band structures and responses to electric fields. A band gap of up to 0.2 eV induced by strong electric fields has been observed in ABC-stacked, with no sign of a band gap opening in ABA-stacked trilayer graphene.[11]

In experiments the field effect is studied by applying a gate voltage V_g between metallic gate electrodes and the graphene sample. The gate electrodes are parallel to the graphene sheet, and the resulting electric field is in the normal direction, see Figs. 1(c,d). Two gate electrodes are employed in some experiments,[9,11] one beneath and the other above the graphene sample, a geometry that is referred as the dual-gate configuration, see Fig. 1(c). The electric fields between the graphene sheet and the two gate electrodes, denoted E_1 and E_2 in the figure, can be controlled by the corresponding gate voltages V_{g1} and V_{g2}. The electric displacements $\epsilon_0 E_1$ and $\epsilon_0 E_2$ can be different, and a difference signals a net charge density σ on the trilayer graphene sheet. In other experimental arrangements[10] there is only a single gate electrode, placed on one side of the graphene sample, the single-gate configuration in Fig. 1(d). In this configuration the electric field between the graphene sheet and the gate electrode is proportional to the net charge density on the graphene trilayer. The single-gate configuration can be considered a special case of the dual-gate configuration with one of the gate voltages equal to zero. In this work we focused on the dual-gate configuration, in which the

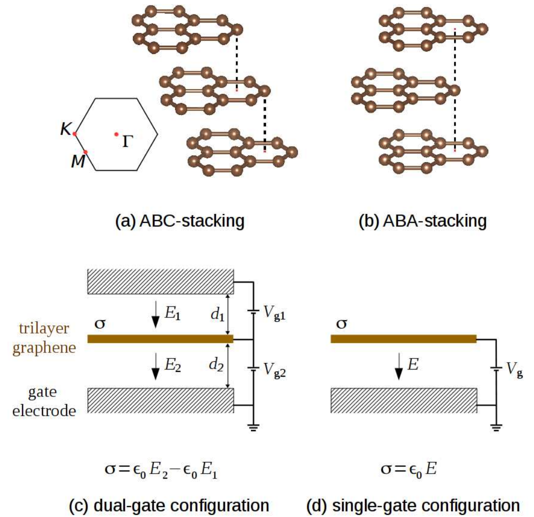

FIG. 1. (Color online) Schematics of the (a) ABC and (b) ABA stacking orders of trilayer graphene, and the (c) dual- and (d) single-gate configurations used in simulations. The first Brillouin zone of trilayer graphene is shown in the insert in (a). In (c,d) the net charge density on the trilayer graphene is denoted by σ, and the electric field between graphene and gate electrodes is denoted by E. Vacuum (permittivity ϵ_0) is used as the medium between graphene and gate electrodes in our simulations.

electric field and charge doping on graphene trilayers can be separately tuned. While the effect of electric field on the electronic structure of trilayer graphene has been the object of many experimental[7–11] and theoretical[10,12–15] studies, the effect of charge doping has received little attention so far.

Theoretical investigations of graphite and of few-layer graphene have relied heavily on empirical tight-binding models,[16–19] which include several intra- and inter-layer off-site hopping terms. Electric field effects on the charge distribution and on on-site energies can be treated using self-consistent Hartree theory.[12,13,20] The empirical tight-binding models have successfully reproduced the electric-field-induced band gap opening for ABC-stacked trilayer graphene;[10,12–14] however, they suffer from the the subtle interactions of the off-site hopping parameters and from the absence of exchange and correlation screening effects.[14] Density functional theory[21,22] (DFT), solving the Kohn-Sham equations self-consistently with a sophisticated approximation for the exchange-correlation functional, in most cases provides a superb description of electronic structure. In this work we employed DFT in conjunction with the effective screening medium[23] (ESM) technique to study electric field effects on ABC- and ABA-stacked trilayer graphene.

The rest of the paper is organized as follows: The DFT method used in our calculations is outlined in Section II. In Section III, we discuss in detail the effects of electric field and charge doping on the electronic structure of ABC- and ABA-stacked trilayer graphene. A final summary is given in Section IV.

II. COMPUTATIONAL METHOD

The band structures of trilayer graphene were calculated using DFT on a plane-wave basis with pseudopotentials and employing the Perdew-Burke-Ernzerhof (PBE) parameterized generalized gradient approximation (GGA) exchange-correlation functional.[24] Graphene trilayers embedded between two semi-infinite media (vacuum or ideal metal) were treated employing the effective screening medium (ESM) method[23] as implemented in the Quantum ESPRESSO package[25]. The methods introduced in Refs. 26–28 treat the single-gate configuration [Fig. 1(d)] by including the electrostatic potentials from fictitious monopole and dipole layers; they are not capable of dealing with the dual-gate configuration shown in Fig. 1(c). The ESM method solves the electrostatic potential by explicitly considering the boundary condition due to the presence of gate electrodes.[23]

The calculated in-plane lattice constant of trilayer graphene using PBE is 2.464 Å, which is equal to the value measured for graphite in experiments.[29] The graphene monolayers are weakly bound by van der Waals interactions. The van der Waals density functional (vdW-DF) theory[30] is employed to treat the weak interlayer interactions. We benchmarked vdW-DF variations on the graphite system, and the results are presented in the Appendix. We chose the vdW-DF with codename "vdw-df2-b86r"[31] as the best among the available vdW-DF variations, although it slightly underestimates the out-of-plane lattice constant of graphite, see the Appendix. The calculated interlayer distance of trilayer graphene using the "vdw-df2-b86r" vdW-DF is 3.342 Å, which is slightly shorter than 3.350 Å than that adopted in previous theoretical work.[14,32] We also performed structural relaxation under a gate voltage using the ESM method, for gate voltages within the same range as used for the electronic structure calculations shown in the results section. We found that the inter-layer distance relaxation is less than 2×10^{-4} Å, and we also confirmed no visible effect on the electronic structure. We chose 3.350 Å as the interlayer distance used to calculate the electronic structure for trilayer graphene.

In experiments the region between the trilayer graphene and the gate electrodes [Figs. 1(c,d)] is filled by dielectric materials such as HfO_2[9] and SiO_2[11]. The high carrier mobility of trilayer graphene on HfO_2 and on SiO_2 substrates[9,33] indicates a weak coupling between the trilayer graphene and these dielectric materials. In our calculations we replace the dielectric material between trilayer graphene and gate electrodes with vacuum. The thickness of vacuum between graphene and gate electrodes is larger than 10 Å, to prevent a charge density overlapping with the gate electrode, a requirement of the ESM method.[23] For self-consistent calculation of the charge density, the first Brillouin zone was sampled by a 55×55 uniform k-mesh with a Methfessel-Paxton[34] smearing of 1 mRy. The convergence threshold for self-consistency is 10^{-10} Ry. The calculation of the density of states (DOS) of graphene systems requires an ultra-fine k-mesh. Since we are interested in the DOS in the vicinity of the Fermi energy, which is contributed by electronic states near the K point in the first Brillouin zone. So we calculated the DOS by integrating over a tiny rhombus whose area is 0.36% of that of the first Brillouin zone, centered at the K point and sampled by a uniform 61×61 k-mesh with a Gaussian smearing of 0.5 mRy.

III. RESULTS

In this section we present calculation results using the dual-gate configuration shown in Fig. 1(c). Results for ABC-stacked trilayer graphene are discussed in subsection A, and for ABA in subsection B. In each subsection, we first discuss the effect of electric fields with the trilayer graphene kept neutral, followed by the dependence of the band structure on the net charge density.

A. ABC-stacked trilayer graphene

At zero electric field the ABC-stacked trilayer graphene is a semi-metal, with the highest valence band touching the lowest conduction band near the K point, as in Fig. 2(a). The band structure at an electric field of $\epsilon_0 E = 0.023\,\mathrm{C/m^2}$ is shown in Fig. 2(b). The energy gap at the K point is then about 0.4 eV, while the energy gap minima at the two points denoted as E_{g1} (along the K-Γ path) and E_{g2} (along the K-M path) are about 0.2 eV. The energy gap on a k-point mesh centered at K-point is shown in pseudo-color in Fig. 2(c). We can see that the k-points with an energy gap close to 0.2 eV form a circle-like region. Note that due to the trigonal warping[14] the K-Γ and K-M paths are inequivalent, leading to the asymmetry in the sizes of V_{g1} and V_{g2} as shown in Fig. 2(d). The energy gaps E_K at the K-point (circles) and E_{g1} and E_{g2} (triangles and squares) are plotted as a function of the electric field in Fig. 2(d). The band gap of about 0.2 eV induced by an electric field of $\epsilon_0 E = 0.02\,\mathrm{C/m^2}$ or larger is in good agreement with a recent experiment.[9]

Projecting the DOS onto each graphene layer helps to understand the mechanism of the energy gap opening. The band structure and the layer-projected DOS at small electric field ($\epsilon_0 E = 0.006\,\mathrm{C/m^2}$) are shown in Fig. 3(b). The flat dispersion in the band structure (left panel) near the energy gap results in two sharp peaks in the DOS. Neither of these peaks is contributed by the central graphene layer (black solid line), but respectively by the graphene layers on the bottom and top of the graphene trilayer; thus, we can attribute the band gap opening as a result of the electric-field-induced potential difference between the bottom and top graphene layers [Fig. 4 inset (a)].

At higher electric fields the peaks in the DOS are no longer contributed solely by one of the graphene layers. At an electric field of $\epsilon_0 E = 0.030\,\mathrm{C/m^2}$ [Fig. 3(e)], the bottom and the top graphene layers contribute almost equally to the two peaks in the DOS, and the central graphene layer also makes a sizable contribution. As a result, the field-induced potential difference can no longer enhance the energy gap. This explains the saturation of field-induced energy gaps at high electric fields [Fig. 2(d)].

We next turn to the effect of charge doping. Charge doping of the trilayer graphene is accompanied by unequal electric fields on the two sides [E_1 and E_2 in Fig. 1(c)]. In this case the electric field is defined as $E = (V_{g1} + V_{g2})/(d_1 + d_2)$. In our calculation we set $d_1 = d_2$, so that $E = (E_1 + E_2)/2$. At zero electric field, the band structure is rigidly shifted by the charge doping. The band gap as a function of the net charge density at finite electric fields is shown in Fig. 4. The energy gaps plotted in Fig. 4 correspond to E_{g1} illustrated in Fig. 2(b), the energy gap along the K-Γ path. At a small electric field of $\epsilon_0 E = 0.006\,\mathrm{C/m^2}$, both electron- and hole-doping of $7.6\times10^{12}\,\mathrm{cm^{-2}}$ can enhance the band gap by about 0.05 eV. The energy gap is unchanged by charge doping at high electric field of $\epsilon_0 E = 0.030\,\mathrm{C/m^2}$.

By comparing the layer-projected DOS in Figs. 3(a-c) and (d-f), we can see that charge doping does not change the distribution of DOS over the three graphene layer,

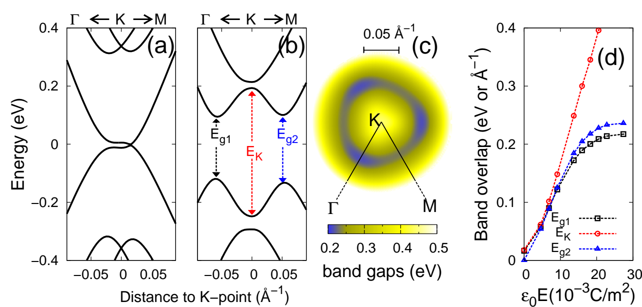

FIG. 2. (Color online) The band structure of ABC-stacked trilayer graphene near the Fermi energy under electric fields (a) $E = 0$ and (b) $\epsilon_0 E = 0.023\,\mathrm{C/m^2}$ with the trilayer graphene kept neutrally charged. The energy gap at the K-point is denoted as E_K, and the smallest band gaps along the Γ–K and Γ–M paths are denoted as E_{g1} and E_{g2} . In (c) the energy gap at electric field of $\epsilon_0 E = 0.023\,\mathrm{C/m^2}$ is plotted on a k-point mesh centered at the K-point. The dependence on the electric field is plotted in (d).

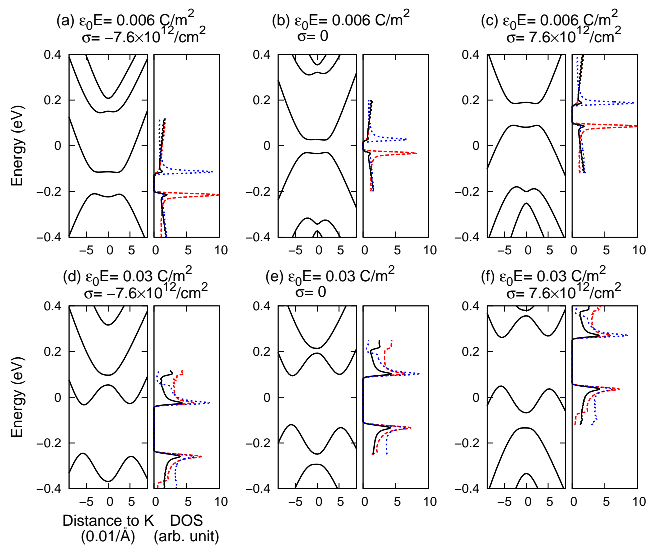

FIG. 3. The band structure (left in each panel) and the density of states (right) of ABC-stacked trilayer graphene are shown for different electric fields and charge dopings. The electric field is $\epsilon_0 E = 0.006\,\mathrm{C/m^2}$ for (a-c), and $\epsilon_0 E = 0.030\,\mathrm{C/m^2}$ for (d-f). The net charge density on the trilayer graphene is $-7.6\times10^{12}\,\mathrm{cm^{-2}}$ for (a,d), zero for (b,e), and $+7.6\times10^{12}\,\mathrm{cm^{-2}}$ for (c,f). The band structure is plotted along the same path as in Figs. 2(a)(b). The layer-projected density of states on the central graphene layer is denoted by solid (black) lines, and on the other two graphene layers by dashed (red) and dotted (blue) lines.

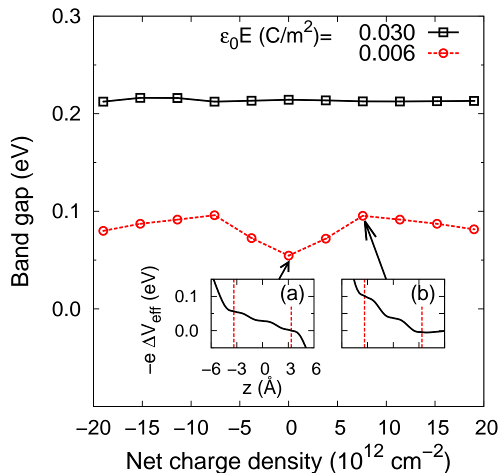

FIG. 4. The band gap of ABC-stacked trilayer graphene as a function of the net charge density. The electric field strength is $\epsilon_0 E = 0.030\,\mathrm{C/m^2}$ (squares) and $\epsilon_0 E = 0.006\,\mathrm{C/m^2}$ (circles). The changes in the potential energy felt by electrons along the direction of the electric field are plotted in the insets, where the positions of the top and bottom graphene layer are denoted by vertical dashed lines.

so the changes in the band gap induced by charge doping can also be attributed to the changes in the potential difference on the top and bottom graphene layers. At an electric field of $\epsilon_0 E = 0.03\,\mathrm{C/m^2}$ the central graphene layer contribute 20–25% of the total density of states according to the values of projected DOS at the band edges shown in Figs. 3(d-f). The potential energy felt by electrons averaged over the x-y plane is plotted along the z-direction in the insets of Fig. 4. At zero doping the potential energy difference between top and bottom graphene layer is 0.05 eV [inset (a)], while hole-doping of $7.6 \times 10^{12}\,\mathrm{cm^{-2}}$ increases the potential energy difference to 0.1 eV [inset (b)]. Accordingly the band gap is enhanced from 0.05 eV at zero doping to 0.1 eV. Another observation from Fig. 4 is the symmetry in the band gap changes for electron and hole dopings. The underlying mechanism is that the shapes of layer-projected DOS are not very sensitive to charge doping. We will see later a different scenario in ABA stacking.

B. ABA-stacked trilayer graphene

The band structure of ABA-stacked trilayer graphene near the Fermi energy consists of two linear monolayer-like bands and two quadratic bilayer-like bands [Fig. 5(a)]. These four bands are strongly hybridized at finite electric fields; two of them overlap near the Fermi energy, while the other two bands are repelled away from the Fermi energy, see Fig. 5(b). The band overlap is illustrated in Fig. 5(c) by a pseudo-color plot of the energy gaps on a mesh of k-points near the K-point. The three-fold rotational symmetry of the ABA-stacked lattice is apparent. The band overlap creates six Dirac-like points with tiny gaps of $\sim 10\,\mathrm{meV}$; three of these are located at the corners and the other three on the edges of a triangle-like region centered at the K-point. The width of the band overlap as measured in k-space (Δk) and in energy space (ΔE) is illustrated in Fig. 5(b). Both Δk and ΔE are increased by electric fields.

The total DOS and the DOS projected on the central graphene layer at $E = 0$ and $\epsilon_0 E = 0.015\,\mathrm{C/m^2}$ are shown in Figs. 6(b) and (e). The layer-projected DOS on the other two graphene layers are almost the same, and so for clarity they are not shown. At $E = 0$ the small band gap between the two quadratic bands near the Fermi energy results in a small dip in the total DOS. The lower edge of the dip is contributed mainly by the central graphene layer. At $\epsilon_0 E = 0.015\,\mathrm{C/m^2}$ the two peaks in the total DOS correspond to the boundaries of the band overlap region. The lower peak is mainly contributed by the central graphene layer. Thus, the band overlap is related to the effective potential of the central graphene layer with respect to the other two layers; this is different from the ABC-stacked case.

At $E = 0$ the effect of charge doping is shown in Figs. 6(a-c). When the graphene trilayer is hole-doped with a net charge density of $9.5 \times 10^{12}\,\mathrm{cm^{-2}}$ [Fig. 6(c)], the edges of the dip in the total DOS develop into two visible peaks, and the gap between the two quadratic bands is enhanced from 0.02 eV to 0.07 eV. At electron-doping [Fig. 6(a)] the contribution of the central graphene layer shifts to the upper edge of the dip. This is due to the higher potential energy felt by electrons at the central graphene layer [Fig. 7 inset (a)]. At an electric field of $\epsilon_0 E = 0.015\,\mathrm{C/m^2}$ the edges of the dip in total DOS develop into clear peaks. Hole doping of $9.5 \times 10^{12}\,\mathrm{cm^{-2}}$ enhances the energy difference between these two peaks and turns the band overlap into a band gap [Fig. 6(f)]. Upon electron doping [Fig. 6(d)], the contribution of the

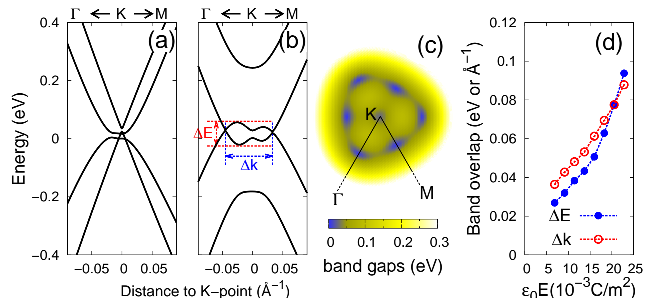

FIG. 5. (color online) The band structure of ABA-stacked trilayer graphene under electric fields of (a) 0 and (b) $0.023\,\mathrm{C/m^2}$, respectively. In (c) the energy gap at electric field of $\epsilon_0 E = 0.023\,\mathrm{C/m^2}$ is plotted on a k-point mesh centered at the K-point. The widths of the band overlaps induced by electric fields marked as Δk and ΔE in (b) are plotted in (d) as a function of the electric field.

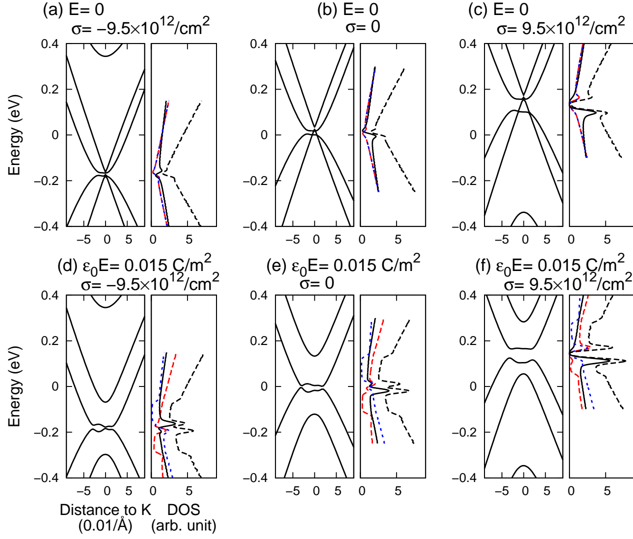

FIG. 6. The band structure (left in each panel) and the density of states (right in each panel) of ABA-stacked trilayer graphene at different electric fields and charge dopings. The electric field is $E = 0$ for (a-c) and $\epsilon_0 E = 0.015\,\mathrm{C/m^2}$ for (d-f). The net charge density on the trilayer graphene is $-9.5 \times 10^{12}\,\mathrm{cm^{-2}}$ for (a,d), 0 for (b,e), and $+9.5 \times 10^{12}\,\mathrm{cm^{-2}}$ for (c,f). The band structure is plotted along the same path as in Figs. 5(a-b). The layer-projected density of states on the central graphene layer is denoted by solid (black) lines, and on the other two graphene layers by dashed (red) and dotted (blue) lines. The total density of states is denoted by dashed black lines.

central graphene layer shifts to the upper peak, reminiscent of the case with zero electric field in Fig. 6(a).

The energy differences between the two peaks in the total DOS at $E = 0$ (squares and black solid line) and $\epsilon_0 E = 0.015\,\mathrm{C/m^2}$ (circles and red dashed line) are plotted as a function of the net charge density in Fig. 7. We can see that the electric field plays only a minor role. The energy difference is larger on the hole-doping side than that for electron doping, which can be attributed to two factors. First, the doping-induced potential difference Δ between the central graphene layer and the other two layers (shown as the solid black lines in the insets of Fig. 7) is larger on the hole-doping side. Second, the central graphene layer always dominates the lower peak in the hole-doping side, which makes the potential difference induced by dole-doping efficiently turn into an energy difference between the two peaks. On the electron-doping side, the potential difference is counteracted by i) the shift of the main contribution of the central graphene layer from the lower peak to the higher peak, and ii) the remaining small contribution to the lower peak [Fig. 6(d)].

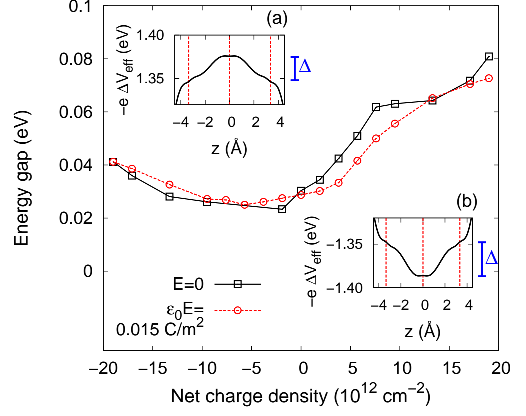

FIG. 7. The energy gap between the two peaks in the total DOS of ABA-stacked trilayer graphene as a function of the net charge density shown for electric field strength $E = 0$ (squares and black solid line) and $\epsilon_0 E = 0.015\,\mathrm{C/m^2}$ (circles and red dashed line). Insets show the changes in the potential energy felt by electrons along the direction of the electric field (black solid lines), where the positions of the graphene layers are denoted by vertical dashed lines.

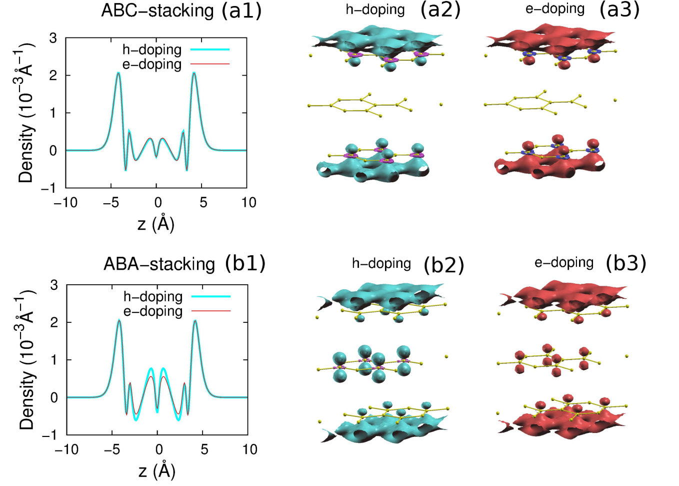

FIG. 8. The density of electrons and holes imposed by gate voltages on (a) ABC-stacked and (b) ABA-stacked trilayer graphene. The net charge density is $-9.5 \times 10^{12}/\mathrm{cm^2}$ for electron doping and $+9.5 \times 10^{12}/\mathrm{cm^2}$ for hole doping. The densities along the z-axis after integrating over the x-y plane are shown in (a1) and (b1). The iso-surface of electron density are shown in (a2, a3) and hole density in (b2, b3); the contour value is set as $\pm 0.05 \times 10^{-3}/\mathrm{\AA}^3$.

C. Electron and hole densities

The electron-hole symmetry in ABC-stacked (Fig. 4) and asymmetry in ABA-stacked trilayer graphene (Fig. 7) can also be illustrated by the spatial distributions of electrons and holes imposed by gate voltage. For

ABC-stacking the hole density on the hole-doping side [Fig. 8 (a2)] is indistinguishable from the electron density on the electron-doping side [Fig. 8 (a3)]. If we further integrate the hole- and electron-density within the x-y plane, the resulting curves are identical along the z-direction [Fig. 8 (a1)]. The electron-hole symmetry apparent in the identical electron and hole densities can be observed for all the conditions in our calculations. For ABA-stacked trilayer graphene the electron-hole asymmetry is equally illustrated by the different distributions of holes [Fig. 8 (b2)] and electrons [Fig. 8 (b3)]. In particular, the hole-density on the central graphene layer is higher than the corresponding electron density, which can also be seen from the z-dependence shown in Fig. 8 (b1).

IV. SUMMARY

The effects of electric field on the electronic structure of trilayer graphene with ABC- and ABA-stacking orders were studied thoroughly using DFT in conjunction with the ESM method. The band gaps or overlaps induced by electric fields in ABC(ABA)-stacked trilayer graphene were fully characterized by results from first-principles calculations. By simulating the dual-gate configuration we are able to look separately at the effects of electric field and those of charge doping. Changes in the band gap of ABC-stacked graphene trilayer are symmetric for hole and electron doping, since the shape of the distribution of layer-projected DOS remains largely unchanged upon charge doping. In contrast, electron and hole dopings cause distinct changes to the electronic structure of ABA-stacked trilayer graphene, reflected in an asymmetrical charge-dependent energy gap curve. The single-gate configuration as shown in Fig. 1 (d) is a special case of the dual-gate configuration, setting V_{g1} and E_1 to zero. In the single-gate configuration the electric field is proportional to the net charge density. From our calculations using the dual-gate configuration, we emphasize that the single-gate field-effect on the band structure arises from both the electric field and the charge-doping.

Our findings are of great importance in guiding future experimental and computational searches aiming to control band structure. Further investigations with the inclusion of spin-orbital couplings are underway.

ACKNOWLEDGMENTS

This work was supported by the US Department of Energy (DOE), Office of Basic Energy Sciences (BES), under Contract No. DE-FG02-02ER45995. Computations were done using the utilities of the National Energy Research Scientific Computing Center (NERSC).

Appendix: Benchmark of van der Waals density functionals on graphite

In this section we report benchmark tests of the effects of variations of the van der Waals density functionals (vdW-DF)[30] implemented in the QUANTUM ESPRESSO package[25] on the structural and elastic properties of graphite. The aim of this benchmark study is to find the optimal functional capable of describing the field effect on the inter-layer distance in graphene trilayers. The lattice constants, the C_{33} elastic constant, and the inter-layer binding energy of graphite are calculated using variations of vdW-DF's. The exchange-correlation energy as a functional of charge density in the vdW-DF theory is

$$E_{\mathrm{xc}}^{\mathrm{vdW-DF}}[n] = E_x^{\mathrm{GGA}}[n] + E_c^{\mathrm{LDA}}[n] + E_{\mathrm{c}}^{\mathrm{nl}}[n]. \quad (\mathrm{A.1})$$

The first term on the right hand side, E_x^{GGA}, is the exchange part of variations of generalized gradient approximation (GGA) functionals. The second term, E_c^{LDA}, is the correlation part of the local density approximation (LDA) functional. The third term, $E_{\mathrm{c}}^{\mathrm{nl}}$, contains variations of the nonlocal part of the correlation, including vdW1[30] and vdW2. The vdW-DF variations tested are listed in Table I.

According to the benchmark results, the vdW-DF's with codename "vdw-df" and "vdw-df2" (see Table I) overestimate both in-plane and out-of-plane lattice constants, but underestimate the C_{33} component of the elastic constant. The remaining six vdW-DF's are almost equally good at predicting the in-plane lattice constant and the C_{33} elastic constant, However, only "vdw-df-obk8" and "vdw-df2-b86r" predict a reasonable out-of-plane lattice constant c_0; the other four underestimate c_0. Comparing "vdw-df-obk8" and "vdw-df2-b86r", we chose "vdw-df2-b86r" since it leads to a inter-layer distance closer to the experimental results.

vdW-DF codename	GGA flavor	non-local scheme	Reference
vdw-df	revPBE	vdW1	Ref. 30
vdw-df2	revised PW86	vdW2	Ref. 35
vdw-df-obk8	optB88	vdW1	Ref. 31
vdw-df-ob86	optB86b	vdW1	Ref. 36
vdw-df-cx	cx	vdW1	Ref. 37
vdw-df-c09	C09x	vdW1	Ref. 38
vdw-df2-c09	C09x	vdW2	Ref. 38
vdw-df2-b86r	revised B86b	vdW2	Ref. 39

TABLE I. The van der Waals density functional (vdW-DF) variations used in the benchmark calculations.

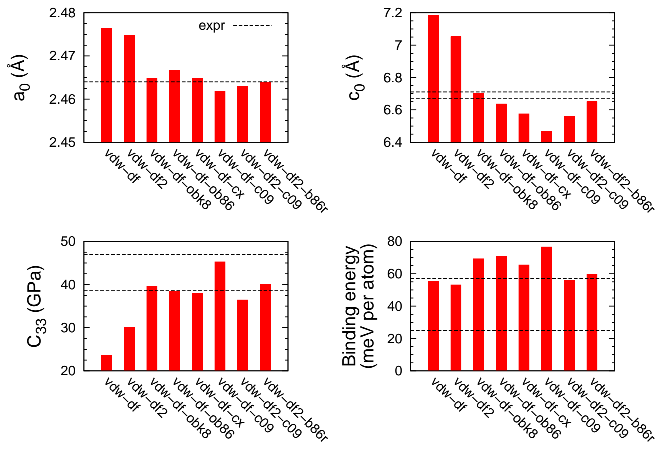

FIG. 9. (a,b) Lattice constants, (c) the C_{33} component of elastic constant, and (d) the interlayer binding energy calculated using variations of van der Waals density functionals listed in Table I. The range of experimental results are denoted by the two black dashed lines, except (a) for which there is no spread. References for the experimental results are: (a) Ref. 29; (b) Refs. 29 and 40; (c) Refs. 41–44 (d) Refs. 43, 45, and 46.

[1] K. S. Novoselov, A. K. Geim, S. V. Morozov, D. Jiang, M. I. Katsnelson, I. V. Grigorieva, S. V. Dubonos, and A. A. Firsov, Nature (London) **438**, 197 (2005).
[2] A. K. Geim and K. S. Novoselov, Nature Mater. **6**, 183 (2007).
[3] F. Schwierz, Nature Nanotechnol. **5**, 487 (2010).
[4] E. McCann, Phys. Rev. B **74**, 161403 (2006).
[5] E. V. Castro, K. S. Novoselov, S. V. Morozov, N. M. R. Peres, J. M. B. L. dos Santos, J. Nilsson, F. Guinea, A. K. Geim, and A. H. C. Neto, Phys. Rev. Lett. **99**, 216802 (2007).
[6] J. B. Oostinga, H. B. Heersche, X. Liu, A. F. Morpurgo, and L. M. K. Vandersypen, Nat. Mater. **7**, 151 (2007).
[7] W. Bao, L. Jing, J. V. Jr., T. Lee, G. Liu, D. Tran, B. Standley, M. Aykol, S. B. Cronin, S. Smirnov, M. Koshino, E. McCann, M. Bockrath, and C. N. Lau, Nat. Phys. **7**, 848 (2011).
[8] E. A. Henriksen, D. Nandi, and J. P. Eisenstein, Phys. Rev. X **2**, 011004 (2012).
[9] K. Zou, F. Zhang, C. Clapp, A. H. MacDonald, and J. Zhu, Nano Lett. **13**, 369 (2013).
[10] C. H. Lui, Z. Li, K. F. Mak, E. Cappelluti, and T. F. Heinz, Nat. Phys. **7**, 944 (2011).
[11] M. Yankowitz, F. Wang, C. N. Lau, and B. J. LeRoy, Phys. Rev. B **87**, 165102 (2013).
[12] A. A. Avetisyan, B. Partoens, and F. M. Peeters, Phys. Rev. B **80**, 195401 (2009).
[13] A. A. Avetisyan, B. Partoens, and F. M. Peeters, Phys. Rev. B **81**, 115432 (2010).
[14] F. Zhang, B. Sahu, H. Min, and A. H. MacDonald, Phys. Rev. B **82**, 035409 (2010).
[15] K. W. Lee and C. E. Lee, Phys. Rev. B **92**, 245416 (2015).
[16] P. R. Wallace, Phys. Rev. **71**, 622 (1947).
[17] J. W. McClure, Phys. Rev. **108**, 612 (1957).
[18] J. C. Slonczewski and P. R. Weiss, Phys. Rev. **109**, 272 (1958).
[19] B. Partoens and F. M. Peeters, Phys. Rev. B **74**, 075404 (2006).
[20] A. A. Avetisyan, B. Partoens, and F. M. Peeters, Phys. Rev. B **79**, 035421 (2009).
[21] P. Hohenberg and W. Kohn, Phys. Rev. **136**, B864 (1964).
[22] W. Kohn and L. J. Sham, Phys. Rev. **140**, A1133 (1965).
[23] M. Otani and O. Sugino, Phys. Rev. B **73**, 115407 (2006).
[24] J. P. Perdew, K. Burke, and M. Ernzerhof, Phys. Rev. Lett. **77**, 3865 (1996).
[25] P. Giannozzi, S. Baroni, N. Bonini, M. Calandra, R. Car, C. Cavazzoni, D. Ceresoli, G. L. Chiarotti, M. Cococcioni, I. Dabo, A. Dal Corso, S. de Gironcoli, S. Fabris, G. Fratesi, R. Gebauer, U. Gerstmann, C. Gougoussis, A. Kokalj, M. Lazzeri, L. Martin-Samos, N. Marzari, F. Mauri, R. Mazzarello, S. Paolini, A. Pasquarello, L. Paulatto, C. Sbraccia, S. Scandolo, G. Sclauzero, A. P. Seitsonen, A. Smogunov, P. Umari, and R. M. Wentzcovitch, J. Phys.: Condens. Matter **21**, 395502 (2009).
[26] T. Brumme, M. Calandra, and F. Mauri, Phys. Rev. B **89**, 245406 (2014).
[27] O. Andreussi, I. Dabo, and N. Marzari, The Journal of Chemical Physics **136**, 064102 (2012).
[28] O. Andreussi and N. Marzari, Phys. Rev. B **90**, 245101 (2014).
[29] P. Trucano and R. Chen, Nature **258**, 136 (1975).
[30] M. Dion, H. Rydberg, E. Schröder, D. C. Langreth, and B. I. Lundqvist, Phys. Rev. Lett. **92**, 246401 (2004).
[31] K. J., B. D. R., and M. A., J. Phys.: Conden. Matter **22**, 022201 (2009).
[32] M. G. Menezes, R. B. Capaz, and S. G. Louie, Phys. Rev. B **89**, 035431 (2014).
[33] W. Zhu, V. Perebeinos, M. Freitag, and P. Avouris, Phys. Rev. B **80**, 235402 (2009).
[34] M. Methfessel and A. T. Paxton, Phys. Rev. B **40**, 3616 (1989).
[35] K. Lee, E. D. Murray, L. Kong, B. I. Lundqvist, and D. C. Langreth, Phys. Rev. B **82**, 081101 (2010).
[36] J. c. v. Klimeš, D. R. Bowler, and A. Michaelides, Phys. Rev. B **83**, 195131 (2011).
[37] K. Berland and P. Hyldgaard, Phys. Rev. B **89**, 035412 (2014).
[38] V. R. Cooper, Phys. Rev. B **81**, 161104 (2010).
[39] I. Hamada, Phys. Rev. B **89**, 121103 (2014).
[40] Y. Baskin and L. Meyer, Phys. Rev. **100**, 544 (1955).
[41] W. B. Gauster and I. J. Fritz, Journal of Applied Physics **45** (1974).
[42] N. Wada, R. Clarke, and S. Solin, The Journal of Chemical Physics **35**, 675 (1980).
[43] L. X. Benedict, N. G. Chopra, M. L. Cohen, A. Zettl, S. G. Louie, and V. H. Crespi, Chemical Physics Letters **286**, 490 (1998).
[44] A. Bosak, M. Krisch, M. Mohr, J. Maultzsch, and C. Thomsen, Phys. Rev. B **75**, 153408 (2007).
[45] L. A. Girifalco and R. A. Lad, The Journal of Chemical Physics **25** (1956).
[46] R. Zacharia, H. Ulbricht, and T. Hertel, Phys. Rev. B **69**, 155406 (2004).